International Colloquium on Jets, Wakes and Shear Layers
Melbourne, Australia, 18-20 April 1994.

INSTABILITIES IN AN IMPINGING JET

K. Hourigan[1], M. Rudman[1] and E. Brocher[2]

[1] CSIRO Division of Building, Construction and Engineering
P.O. Box 56, Highett 3190, Australia

[2] Institut de Mecanique des Fluides de Marseille de l'Universite d'Aix-Marseille II,
U.M. 34 - C.N.R.S., 1, rue Honnorat - 13003 Marseille, France

ABSTRACT

The instabilities in a supersonic impinging jet are investigated by solving the two-dimensional Euler equations using the piecewise parabolic method (PPM) and Roe's linearised Riemann-solver. The frequency and nature of the dominant instabilities are found to be a function of the impingement distance. Two instability modes are possible, a symmetric (or varicose mode) and an asymmetric (or sinuous) mode. For a given jet exit Mach number (M = 1.29 here), the energy in, and frequency of, these modes are a function of impingement distance, leading to an integral staging due to an acoustic feedback loop.

Nomenclature

a	= ambient sound speed	U	= state vector of the flow
d	= jet nozzle width	v	= velocity in transverse direction
e	= E - 1/2(u^2+v^2), internal energy/unit mass	V_c	= average convection velocity
E	= total energy/unit volume	V_L	= loop velocity, $V_c/(1 + V_c/a)$
f	= frequency of impingement tone	V_1	= jet exit velocity
h	= distance between nozzle and wall	x	= axial distance
L	= shock cell length	y	= transverse distance
M_1	= jet exit Mach number = 1.29		
n	= number of periods of sound wave in feedback loop	α	= ratio of convection to jet exit velocities
p	= pressure	ρ	= local fluid density
u	= velocity in axial direction		

INTRODUCTION

Below a jet Mach number of 0.6, no tones are observed for cold jets impinging normally to a wall. The strong tones emitted when high subsonic or supersonic jets impinge normal to a wall have been found to contain frequency jumps as the distance to the wall is varied gradually (Wagner 1971, Neuwerth 1974). This staging effect is characteristic of systems driven by an acoustic feedback. For round impinging subsonic jets, Neuwerth identified the feedback acoustic disturbances inside the jet column through analysis of high-speed movies. Ho and Nossier (1981) investigated the feedback loop and the associated acoustic tones for subsonic impinging jets.

In round jets, the allowable frequencies of the helical neutral wave modes that propagate upstream are too high to match those of the instability waves of the jet at subsonic Mach numbers. At supersonic Mach number, frequency matching becomes possible; the stable helical feedback loop and the generation of impingement tones can be maintained. Tam and Ahuja (1990) proposed that the feedback was achieved by a family of upstream propagating acoustic waves of the jet flow (see Fig. 1). For subsonic jets, these waves can exist inside the jet; for the supersonic case, the acoustic waves are restricted to travelling upstream outside of the jet. In the subsonic case, the instability waves in the jet were invariably axisymmetric whereas in the supersonic case, both axisymmetric and helical modes were observed. Tam and Ahuja were able to predict the average impingement tone frequency at different jet Mach numbers and also explain why no tones were observed for cold jets for Mach numbers less than 0.6.

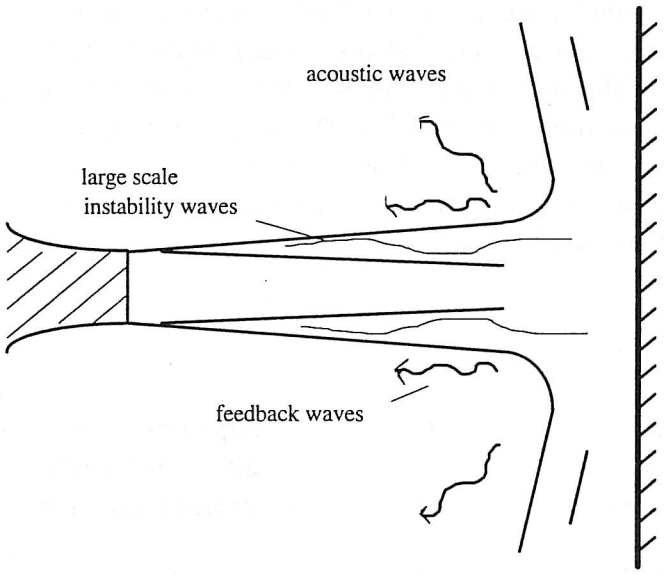

Figure 1. Schematic of the feedback loop of an impinging jet.

In supersonic rectangular jets, although the noise spectrum consists of many tones, there are only two basic tone frequencies (Tam and Norum 1992). The basic frequency associated with an antisymmetric mode is higher than the basic tone associated with a symmetric tone. All of the other tones in the spectrum are found to be combination tones of the two basic tones and their harmonics and are generated by the nonlinearities of the jet flow.

In this paper, we model the impingement process for a supersonic 2 dimensional using the Piecewise Parabolic Method, with the aim of understanding the mechanisms involved in the feedback process.

NUMERICAL METHOD

In cartesian space variables, x and y, the two-dimensional equations of compressible hydrodynamics, written in conservation form, are:

$$\frac{\partial U}{\partial t} + \frac{\partial F(U)}{\partial x} + \frac{\partial G(U)}{\rho \partial y} = 0$$

(1)

where

$$U = \begin{pmatrix} \rho \\ \rho u \\ \rho v \\ \rho E \end{pmatrix}, \quad F(U) = \begin{pmatrix} \rho u \\ \rho u^2 + p \\ \rho uv \\ (\rho E + p)u \end{pmatrix}, \quad G(U) = \begin{pmatrix} \rho v \\ \rho v \\ (\rho E + p)v \\ 0 \end{pmatrix}$$

(2)

Equation (1) is solved by decomposition into two one-dimensional hyperbolic problems:

$$L_x \text{ solves } \frac{\partial u}{\partial t} + \frac{\partial F(U)}{\partial x} = 0, \; L_y \text{ solves } \frac{\partial u}{\partial t} + \frac{\partial G(U)}{\partial y} = 0$$

(3)

The combined solution is computed as follows:

$$U^{n+2} = L_x L_y L_x L_y U^n$$

(4)

Here, u is the component of the velocity in the direction of the one-dimensional sweep, v is the velocity orthogonal to u, ρ is the density, p is the pressure, E is the total energy per unit volume, e is the internal energy per unit mass defined to be $E - 1/2(u^2 + v^2)$.
The PPM scheme is a characteristic-based method and a higher-order extension of Godunov's method (Godunov 1959) as developed by Colella and Woodward (1984). The PPM algorithm defines an interpolation function of the primitive variables $v_i \in \{\rho, u, v, p\}$, which is parabolic over each cell. Monotonicity of the interpolation function is enforced and the piecewise linear parabolic interpolation is replaced near contact discontinuities with a piecewise linear distribution.

Flow variables can then be decomposed into three linearised (x,t) wave characteristics corresponding to upstream, where allowable, and downstream travelling pressure waves and convective transport by the flow. The decomposition is then written in terms of the

amplitudes and eigenvectors of the linear waves, and the desired time average computed as a space average. Roe's linearised Riemman solver is then applied to the corresponding state vectors of conservative variables, and the flow linearised about the Roe average. The scheme is fourth order in time and in space where the solution is smooth and third order in time near discontinuities.

Boundary Conditions:

Inflow: All flow variables are specified at the inflow boundaries. For the jet, the inflow velocity profile is given by:

$$u(y) = \frac{V_1}{2}(1 - \tanh(6.25(\frac{|y|}{d} + \frac{d}{|y|})))$$

(5)

where V_1 is the speed at the centre of the jet at exit and d is the jet width.

Outflow: All (x,t) characteristics are directed outwards and the flow depends neither physically nor numerically on the outflow boundary values.

Grid: A uniform grid was used for each simulation. Figure 2 shows a typical boundary domain with associated boundary conditions.

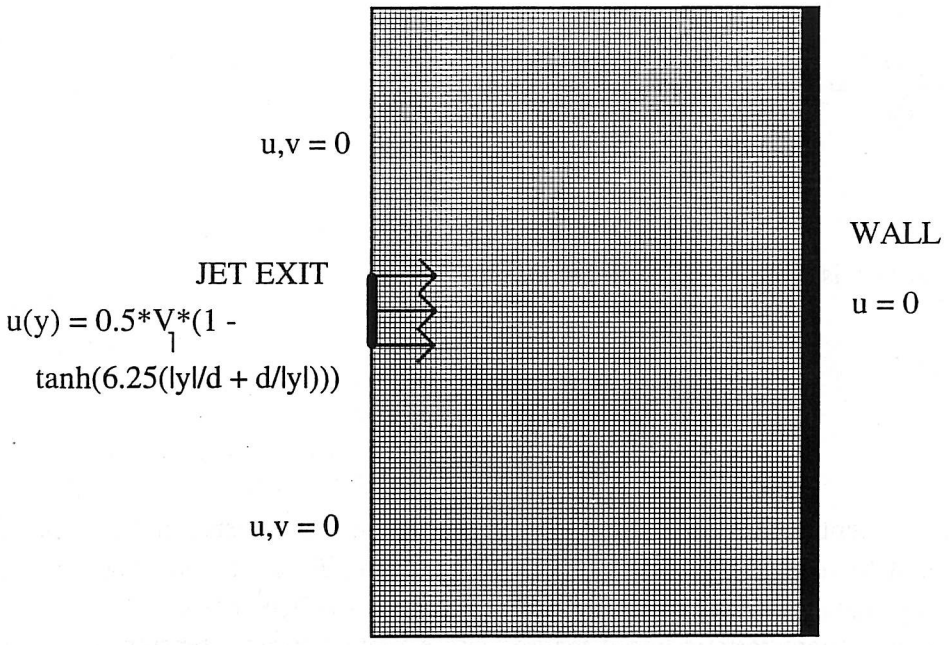

Figure 2. Schematic of a typical mesh used for a simulation of the impinging jet.

RESULTS AND DISCUSSION

The code has been used to model the time-dependent impinging jet over a range of impingement distances for a jet exit Mach number 1.29. A key requirement in the simulations is ensuring that grid resolution is high enough to capture the smallest scales of motion involved in the feedback loop. The code was tested for sensitivity of the predicted frequencies of jet instabilities for a number of grid resolutions. Increasing from a grid size of 128x64 to

256x128, the major spike in the spectra remained at the same frequency (increasing only slightly in energy), indicating that satisfactory resolution had been achieved. For a smaller grid of 64x32, the higher frequency spike had relatively small energy indicating lack of resolution. The largest grid is used in all of the results presented here.

The predicted instantaneous flow for the impingement distance h/d = 6.0 is shown in Fig. 3 in the form of a pseudo-Schlieren plot and a velocity vector field. The code has captured weak shock cells near the jet exit. Sound waves are seen emanating from the impingement region. The large scale instabilities in the jet are also prominent. From the videotapes of these simulations, to be shown at the Colloquium, the sound waves travel outside the jet and interact with the shear layers near the jet exit. Due to the supersonic nature of the jet, the sound waves are unable to reach the jet exit from within the jet.

Figure 3(a). **Plot of predicted instantaneous flow (Schlieren representation) at impingement distance of h/d = 6.0 (flow entering from left, M = 1.29).**

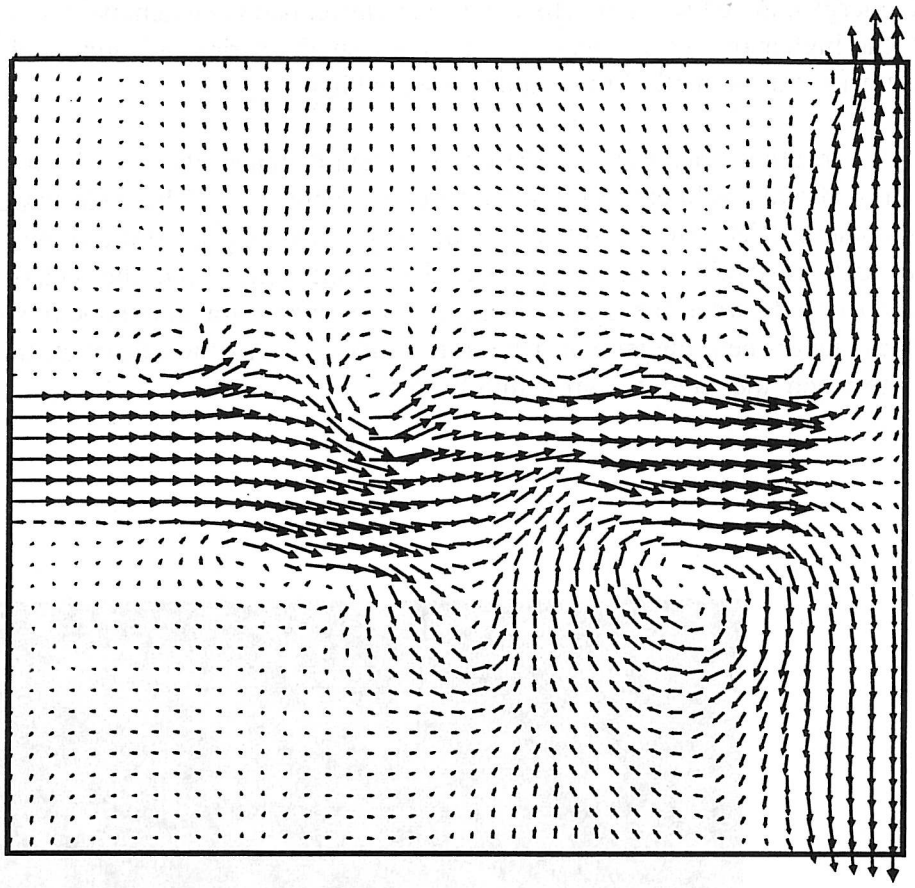

Figure 3(b). Plot of predicted instantaneous velocity vectors at impingement distance of h/d = 6.0 (flow entering from left, only every third vector in each direction plotted, same instant as Fig. 3(a), M = 1.29) .

The power spectra for different impingement distances are shown in Fig. 4. The frequency and magnitude of the dominant peaks is dependent on the impingement distance. Two numerical probes were used to measure the pressure fluctuations on each side of the jet exit. The transfer function enabled the distinction between symmetric and asymmetric modes. The number of impingement tones and their frequencies are clearly a function of the impingement distance.

In terms of a simple feedback model, the feedback loop consists of acoustic waves travelling outside the jet at the ambient speed of sound, a, and triggering, at the receptive nozzle exit, jet instabilities that convect downstream with mean velocity $V_c = \alpha V_L$. The half length of the feedback loop is the impingement distance h. The loop Strouhal number, St_L, is defined as fh/V_L, where $V_L = V_c/(1 + V_c/a)$ is the loop velocity. When the feedback loop is operating, there will be an integral number, n, of waves in the feedback loop, i.e. $St_L = n$.

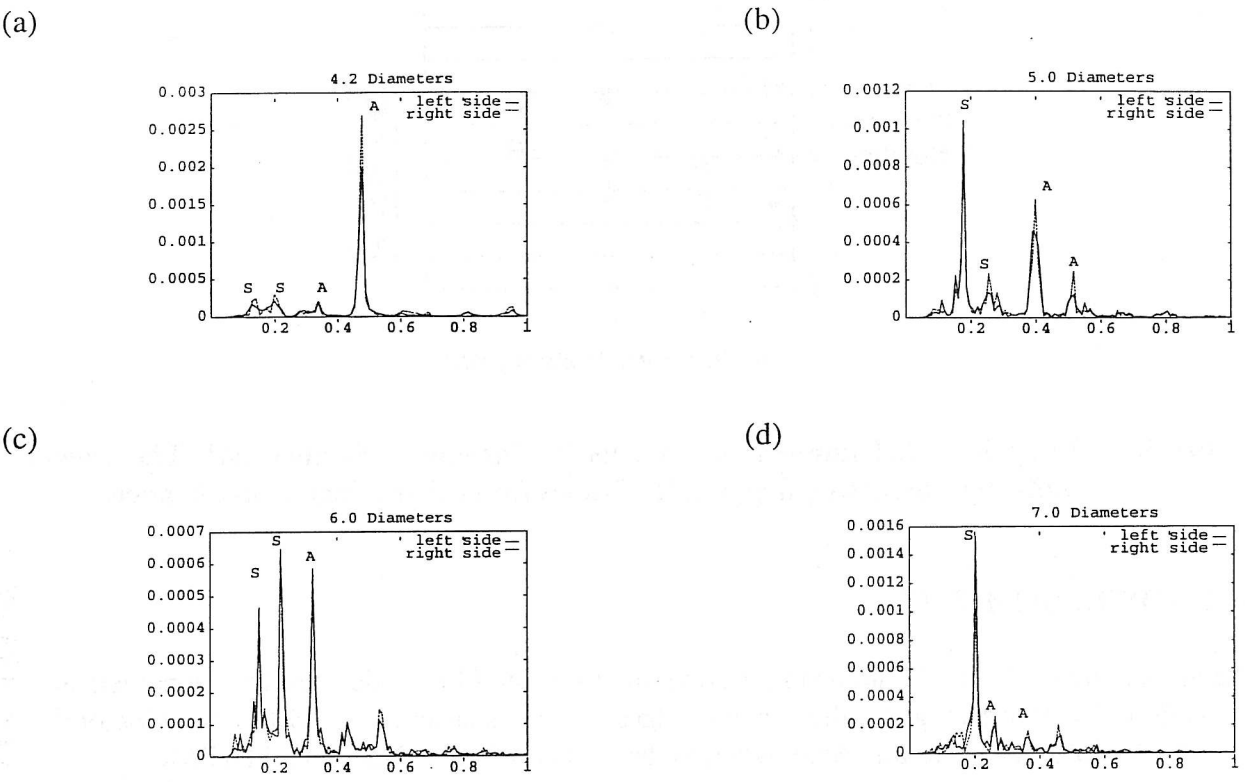

Figure 4. **Power spectra (arbitrary units) for different impingement distances: (a) *h/d* = 4.2; (b) *h/d* = 5.0; (c) *h/d* = 6.0; (d) *h/d* =7.0. Left and right side refers to the position of numerical probes relative to the jet exit. `A' denotes an asymmetric mode, `S' denotes a symmetric mode.**

In Fig. 5, plots of the loop Strouhal number variation of the strongest tones with impingement distance are shown. Here, best fit is obtained for $\alpha = 0.58$, which is in the range 0.53 to 0.62 used by other researchers. The symbols indicate the relative magnitude of the spectral peaks for each impingement distance. Staging of the impingement tones generally into integral values of the loop Strouhal number is observed, indicating that a feedback loop is operating.

For each impingement distance, the lowest frequency impingement tones was due to a symmetric mode. This is in line with the theoretical analysis of Tam and Norum (1992), who determined that the first symmetric mode was always lower in frequency than the first asymmetric mode, and observed in their experiments.

The results of the numerical model are in general agreement with those observed by Norum (1991). Differences arise due to the presence of strong shocks in the experiments, leading to the significant influence of the screech tone. The initial set of results presented here indicates that the code is capable of providing useful insights into the coupling of impingement tones and jet instabilities. It is intended that the study be extended in future to a wider range of impingement distances and different jet exit Mach numbers.

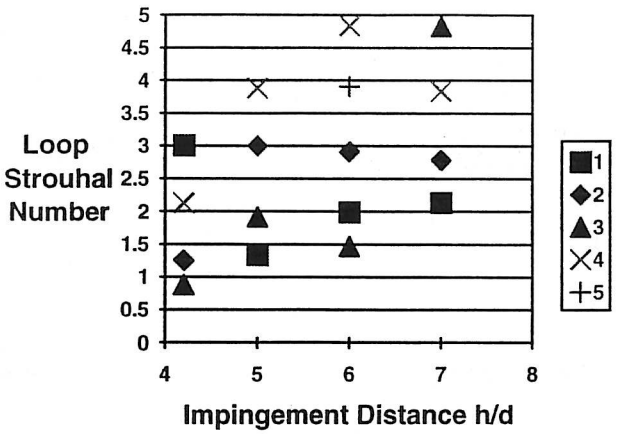

Figure 5. Loop Strouhal number St_l versus impingement distance h/d. The legend indicates decreasing magnitude of tones for each impingement distance.

ACKNOWLEDGMENTS

The authors thank Dr Ralf Gathmann for providing the basic PPM code used for the numerical simulation. Dr Rudman gratefully acknowledges the assistance of a CSIRO Postdoctoral Award. Dr Hourigan gratefully acknowledges the support of the C.N.R.S. and DITARD.

REFERENCES

Colella, P. and Woodward, P.R., ``The Piecewise Parabolic Method (PPM) for gas-dynamical Simulations", Journal of Computational Physics, Vol. 54, 1984, pp. 174-201.

Gathmann, R., ``Analyse d'ecoulements supersoniques et reactifs par simulation numerique instationaire tridimensionelle", PhD thesis, Institut de Mecanique de Grenoble, 1993.

Ho, C.M. and Nossier, N.S., ``Dynamics of an Impinging Jet. Part I. The Feedback Phenomenon", Journal of Fluid Mechanics, Vol. 105, 1981, pp. 119-142.

Nossier, N.S. and Ho, C.M., ``Dynamics of an Impinging Jet. Part II. The Noise Generation", Journal of Fluid Mechanics, Vol. 105, 1981, pp. 379-391.

Neuwerth, G., ``Acoustic Feedback of a Subsonic and Supersonic Free Jet which Impinges on an Obstacle", NASA TT F-15719, 1974.

Norum, T.D., ``Supersonic Rectangular Jet Impingement Noise Experiments", AIAA-89-1138, 1989, pp. 1-12.

Roe, P.L., ``Approximate Riemann Solvers, Parameter Vectors and Difference Schemes", Journal of Computational Physics, Vol. 43, 1981, pp. 357-372.

Tam, C.K.W. and Ahuja, K.K., ``Theoretical Model of Discrete Tone Generation by Impinging Jets", Journal of Fluid Mechanics, Vol. 214, 1990, pp. 67-87.

Tam, C.K.W. and Norum, T.D., ``Impingement Tones of Large Aspect Ratio Supersonic Jets", AIAA Journal, Vol. 30, No. 2, February 1992, pp. 304-311.

Wagner, F.R., ``The Sound and Flow Field of an Axially Symmetric Free Jet upon Impact on a Wall", NASA TT F-13942, 1971.